

One-Step Selective Aerobic Oxidation of Amines to Imines by Gold Nanoparticle-Loaded Rutile Titanium(IV) Oxide Plasmon Photocatalyst

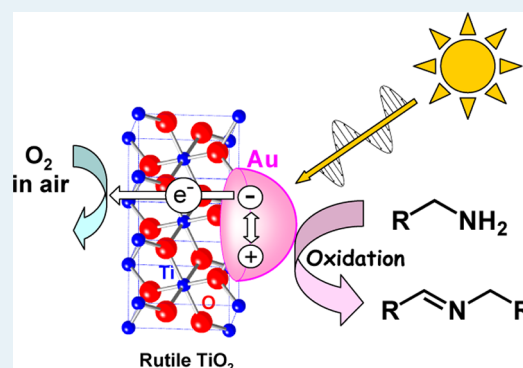
Shin-ichi Naya,[†] Keisuke Kimura,[‡] and Hiroaki Tada^{†,‡,*}

[†]Environmental Research Laboratory, Kinki University, 3-4-1, Kowakae, Higashi-Osaka, Osaka 577-8502, Japan

[‡]Department of Applied Chemistry, School of Science and Engineering, Kinki University, 3-4-1, Kowakae, Higashi-Osaka, Osaka 577-8502, Japan

Supporting Information

ABSTRACT: Among various metal oxide-supported Au nanoparticles, Au/rutile TiO₂ exhibits a particularly high level of visible-light activity for aerobic oxidation of amines to yield the corresponding imines on a synthetic scale with high selectivity (>99%) at 298 K. Experimental results have suggested that the reaction proceeds via the localized surface plasmon resonance-excited electron transfer from the Au nanoparticle to the TiO₂.



KEYWORDS: localized surface plasmon resonance, visible light photocatalysis, Au nanoparticle, selective oxidation, imine synthesis

Imines are important versatile intermediates for fine chemicals and pharmaceuticals and also are applied for mass products, such as dyes.¹ Imines can be synthesized by direct oxidation of amines or condensation of amine with aldehyde.² Several procedures use the stoichiometric amount of harmful or explosive reagents with emission of the corresponding amount of pollutants.^{3,4} The energy and environmental issue requires the development of “green” catalytic processes to oxidize amines efficiently and selectively under mild conditions.^{5,6} Our basic strategy for the reaction design is to use (i) molecular oxygen in air as an oxidizing agent, (ii) no solvent or nontoxic solvent, and (iii) sunlight as an energy source. To achieve this, a new type of photocatalysts consisting of Au nanoparticles (NPs) and metal oxide supports, called “plasmon photocatalysts”, are highly promising^{7–15} because of the possible effective utilization of sunlight as an energy source and their nontoxicity. Although plasmon photocatalysts have recently attracted much attention,¹⁶ studies on organic synthesis are limited to only the oxidations of alcohols to carbonyl compounds,^{17–19} thiols to disulfides,²⁰ and benzene to phenols.^{21,22} On the other hand, the rational material design of highly active plasmon photocatalysts should urge further development of this hot research field. To increase fundamental understanding, the correlation between the photocatalytic activity and the key factors, including the Au particle size^{17,23} and the kind of metal oxide supports,^{13,23} should be clarified.

Here, we show that Au/rutile TiO₂ plasmon photocatalyst exhibits a particularly high visible-light activity for selective

aerobic oxidation of amines to imines with a maximum at Au particle size of ~7 nm at 298 K. The photocatalytic activity can depend on the Au loading amount as well as its particle size. To vary the Au particle size (d) with its loading amount maintained constant, Au NPs were loaded onto various metal oxides (anatase and rutile TiO₂, SrTiO₃, ZnO, WO₃, In₂O₃, Nb₂O₅) by the heating temperature-varied deposition precipitation method (Table S1, see Supporting Information).²⁴ Figure 1 shows transmission electron micrographs of several Au NP-loaded metal oxides (Au/MOs) (see Supporting Information Figure S1 for the other samples). Apparently, Au NPs are highly dispersed on the metal oxide surface in every sample. Table 1 summarizes characterization results of the Au/MOs. The mean Au particle sizes (d /nm) of Au/MOs increase with increases in heating temperature (T_c) and time (t_c). Figure 2 shows UV–vis absorption spectra of Au/MOs, and that of Au colloid is shown for comparison. Au/MO has broad absorption due to the localized surface plasmon resonance (LSPR) of Au NPs, whose peak position depends on the metal oxide support. The LSPR peak position greatly depends on the surrounding permittivity. The significant red-shift of the LSPR peak of Au/rutile TiO₂ results from its very large permittivity ($\epsilon = 114$) as compared with that of anatase TiO₂ ($\epsilon = 48$).²⁵ The LSPR

Received: October 21, 2012

Revised: November 23, 2012

Published: November 26, 2012

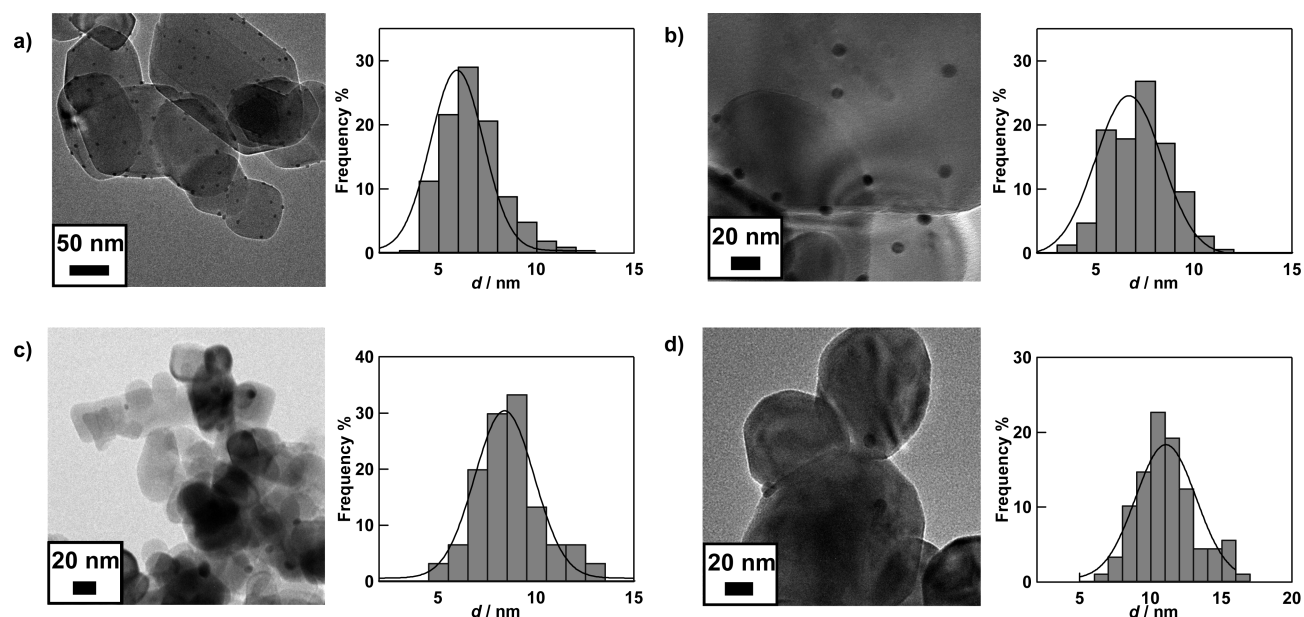


Figure 1. TEM image and size distribution: (a) Au/rutile TiO₂ ($d = 6.7$ nm), (b) Au/anatase TiO₂ ($d = 7.1$ nm), (c) Au/SrTiO₃ ($d = 8.4$ nm), (d) Au/WO₃ ($d = 11.8$ nm).

Table 1. Au Loading Amount; Au Particle Size, d ; Standard Deviation, σ ; Number of Count; Heating Temperature, T_c ; and Time, t_c for the Deposition–Precipitation Method

catalyst	Au mass %	d /nm	σ /nm	count	T_c /K	t_c /h
Au/rutile TiO ₂	0.56	3.5	0.8	248	773	4
Au/rutile TiO ₂	0.56	5.0	1.1	250	803	4
Au/rutile TiO ₂	0.56	6.7	1.5	203	823	4
Au/rutile TiO ₂	0.56	9.7	1.9	298	873	4
Au/rutile TiO ₂	0.56	14.3	2.9	198	873	24
Au/anatase TiO ₂	0.42	3.6	0.6	162	673	4
Au/anatase TiO ₂	0.42	7.1	1.5	145	773	4
Au/anatase TiO ₂	0.42	9.8	1.6	120	873	4
Au/anatase TiO ₂	0.42	12.3	3.6	122	873	24
Au/SrTiO ₃	0.62	2.7	0.6	128	673	4
Au/SrTiO ₃	0.61	3.9	1.2	111	773	4
Au/SrTiO ₃	0.63	8.4	1.9	133	873	24
Au/WO ₃	0.28	11.8	2.1	88	873	4
Au/ZnO	0.31	7.3	1.7	169	773	4
Au/Nb ₂ O ₅	0.30	6.7	2.0	106	873	4
Au/In ₂ O ₃	0.78	11.0	1.8	92	873	4

absorption of most Au/MOs as well as the Au colloid possesses asymmetric character, that is, the absorption intensifies at the shorter wavelength side of the peak. On the other hand, the LSPR absorption profiles for Au/rutile TiO₂, Au/SrTiO₃, and Au/WO₃ are relatively symmetric and in good agreement with that of the solar spectrum.

As shown in Table 2, visible-light irradiation ($\lambda > 430$ nm) to Au/rutile TiO₂ in neat benzylamine (PhCH₂NH₂) yields benzylidenebenzylamine (Ph–CH=N–CH₂Ph) as a single product at 298 K. Intermediate Ph–CH=NH reacts with PhCH₂NH₂ to generate Ph–CH=N–CH₂Ph. At an irradiation time of 24 h, the amount of Ph–CH=N–CH₂Ph reaches 1.06 mmol (4.5%). The turnover number (TON = the molecule number of the imine generated/the number of Au surface atoms) exceeds 5000. In addition, Au/rutile TiO₂ shows high levels of visible-light activity for the oxidations of several

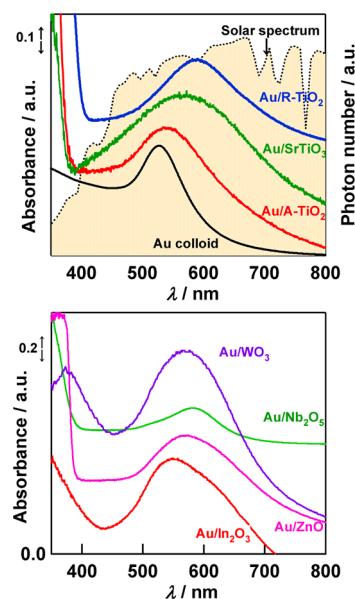
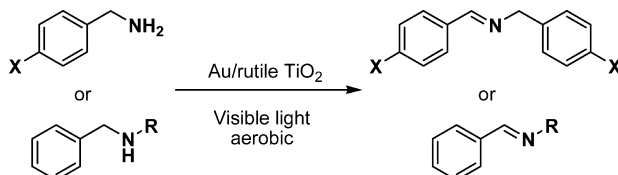


Figure 2. UV–vis absorption spectra of Au/MOs and Au colloid. Rutile and anatase TiO₂ are abbreviated as R-TiO₂ and A-TiO₂, respectively.

other primary and secondary amines to afford the corresponding imines with selectivity >99%.

As described later, photoelectrochemical and adsorption experiments provide important information about the reaction mechanism. The oxidation of benzylamine was also carried out for a 0.1 mM acetonitrile solution. We selected acetonitrile as a solvent because of its excellent electrochemical stability, large dielectric constant, and low toxicity. In this case, benzaldehyde is generated as a major product, with Ph–CH=N–CH₂Ph as a minor product due to the hydrolysis of Ph–CH=NH by water involved in acetonitrile (Supporting Information Table S2).

First, the metal oxide support effect on the photocatalytic activity was examined in the acetonitrile solution. Figure 3A shows time courses for the benzaldehyde generation.

Table 2. Amine Oxidation by Au/Rutile TiO₂^a


amine	yield/mmol	conversion, %	selectivity, %	TON
X = H	1.06	4.5	>99	5.7 × 10 ³
X = Me	0.43	2.1	>99	2.3 × 10 ³
X = Cl	0.12	0.7	>99	6.5 × 10 ²
X = OMe	0.49	2.7	>99	2.6 × 10 ³
R = Me	0.03	0.1	>99	1.7 × 10 ²
R = CH ₂ Ph	0.09	0.3	>99	4.7 × 10 ²

^aVisible-light irradiation ($\lambda > 430$ nm) for 24 h.

Surprisingly, among the various Au/MOs, Au/rutile TiO₂ shows a particularly high level of visible-light activity for the amine oxidation. Zhao and co-workers have recently reported the TiO₂-photocatalyzed oxidation of amines to imines under visible-light irradiation via a surface complex mechanism.²⁶ The activity of Au/rutile TiO₂ is much greater than that of TiO₂ under the same conditions. Au NP loading, visible-light irradiation, and O₂ were necessary for the reaction to be sustained (Supporting Information Figure S2).

Second, the Au particle size effect on the amine oxidation in the acetonitrile solution was studied for the Au/rutile TiO₂, Au/anatase TiO₂, and Au/SrTiO₃ systems. Regardless of the Au particle size, the aldehyde and imine were selectively produced. Figure 3B shows plots of the turnover number (TON = the molecule number of the sum of aldehyde and imine generated/the number of Au surface atoms) at an irradiation time of 1 h as a function of d . The plot for the Au/rutile TiO₂ system shows a volcano-shaped curve with a maximum at $d \approx 6.7$ nm, whereas in the Au/anatase TiO₂ and Au/SrTiO₃ systems, the TONs slightly increase with increasing d .

In addition, the visible-light activity of Au/rutile TiO₂ was examined for the oxidations of several other primary and secondary amines in the acetonitrile solutions (Supporting Information Table S2). The oxidation for every amine yields the corresponding aldehyde and imine with 86–99% conversion at an irradiation time of 24 h. Interestingly, the plot of the initial reaction rate (v_0) vs the oxidation potential of the primary amines (E_{ox}/V vs standard hydrogen electrode, SHE) shows a linear relation with a negative slope (Figure 3C).

This finding suggests that these oxidations proceed via the electron transfer from the amines to Au/rutile TiO₂.

To clarify the origin for the striking support effect, the reaction mechanism was investigated by photoelectrochemical measurements. Au NP-loaded mesoporous rutile TiO₂ nanocrystalline films were formed on the surfaces of fluorine-doped SnO₂ electrodes (Au/mp-rutile TiO₂/FTO), and the electrode potential (E) change induced by irradiation of monochromatic light was measured (Supporting Information Figure S3).⁹ Visible-light irradiation of the electrode in an electrolyte solution containing benzylamine causes a negative shift in E , which hardly changed without benzylamine. Figure 4A

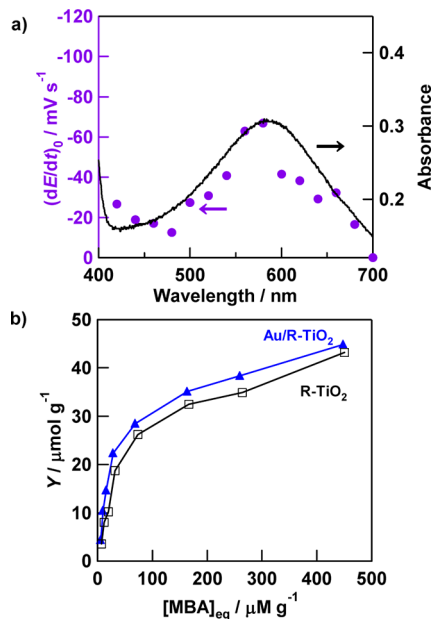


Figure 4. (a) Action spectrum of $(dE/dt)_0$ (violet circle) and diffuse reflectance UV-vis spectrum of Au/mp-rutile TiO₂ (solid line). (b) Adsorption isotherms of 4-methoxybenzylamine (MBA) on rutile TiO₂ (open square) and Au/rutile TiO₂ ($d = 5.0$ nm, blue triangle) at 275 K.

compares the action spectrum of the initial rate of the electrode potential change $(dE/dt)_0$ and the absorption spectrum of Au/mp-rutile TiO₂/FTO. The good resemblance of the profiles indicates that the excitation of the Au NP-LSPR is the driving force for the amine oxidation. The potential upward shift can result from the electron transfer from benzylamine to TiO₂ via LSPR-excited Au NPs. The surface

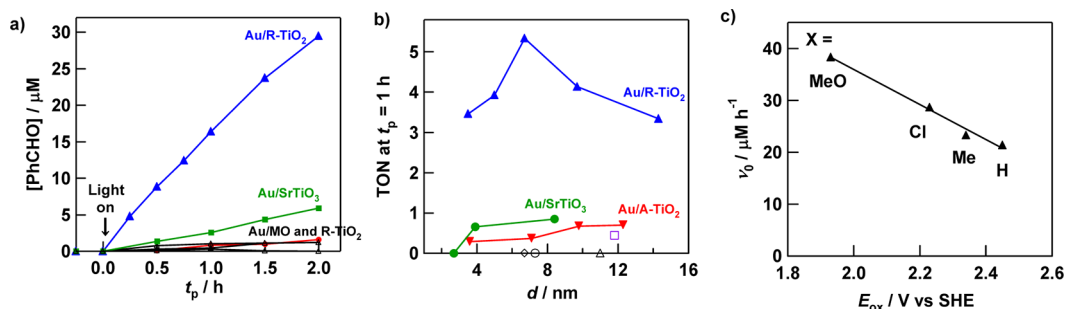


Figure 3. (a) Time course of [PhCHO] generated. (b) TON at $t_p = 1$ h for amine oxidation as a function of Au size d : Au/ZnO (open circle), Au/Nb₂O₅ (open rhombus), Au/In₂O₃ (open triangle), Au/WO₃ (open square). (c) Initial oxidation rate of 4-substituted benzylamine ($X-C_6H_4-CH_2NH_2$) as a function of their oxidation potential (E_{ox}).

complex between benzylamine and TiO₂ has very weak featureless absorption in the visible region.²⁶ Consequently, the Au/rutile TiO₂-photocatalyzed amine oxidation is mainly induced not by the surface complex excitation but probably by the LSPR-excited electron transfer.

The effect of Au NP loading on the adsorption property of rutile TiO₂ for amine was also examined. Figure 4B compares the adsorption isotherms for 4-methoxybenzylamine on rutile TiO₂ and Au/rutile TiO₂ at 275 K: *Y* denotes the equilibrium adsorption amount per unit mass of the solid. Rutile TiO₂ has good adsorptivity for 4-methoxybenzylamine. Diffuse reflectance infrared spectroscopy using pyridine as a probe molecule has suggested the presence of acid sites on the surface of rutile TiO₂.²⁷ 4-Methoxybenzylamine would be adsorbed on the rutile TiO₂ surface by the acid–base interaction. In addition, loading a small amount of Au NP further increases the adsorption amount by $\sim 3 \mu\text{mol g}^{-1}$. At a Au loading amount of 0.56 mass % and *d* of 5.0 nm, the surface area of Au NPs on rutile TiO₂ occupies only $\sim 2\%$ of the total surface area. This fact means that the amine is adsorbed on the surface of the Au NP in preference to rutile TiO₂. A recent density functional theory study has shown that amine is adsorbed on under-coordinated sites of the Au(111) surface via a donation/back-donation mechanism.²⁸

On the basis of these results, we can explain the essential mechanism and the high selectivity of this reaction as follows: In the anodic process, the LSPR-excited electron transfer from Au NP to rutile TiO₂ lowers the Fermi level of Au NPs, which entails the oxidation ability of the Au NPs.²³ Owing to the mild oxidation ability, amines strongly adsorbed on the Au surface are efficiently oxidized to imines without overoxidation. In the cathodic process, O₂ is possibly reduced by the electrons in the conduction band (CB) of rutile TiO₂, since the CB edge (-0.05 V vs SHE)²⁹ is close to the one-electron O₂ reduction potential ($E^0(\text{O}_2/\text{HO}_2) = -0.046 \text{ V}$).³⁰ The amine oxidation is drastically enhanced with addition of Ag⁺ ions as a sacrificial electron acceptor under deaerated conditions (Supporting Information Figure S2). This fact indicates that the O₂ reduction is the rate-determining step in this reaction. On the other hand, the CB edge of WO₃ ($+0.50 \text{ V vs SHE}$) is too low for the O₂ reduction to occur.³¹ In this manner, the mechanism involving the electron transfer from MOs to O₂ can also explain the reason for the lower activity of Au/WO₃. As reported in the preceding paper, the activity of Au/rutile TiO₂, which is superior to that of Au/anatase TiO₂, stems mainly from the efficient electron transfer from Au NP to TiO₂ because of the optical decoupling between the LSPR and the interband transition of Au NPs.²¹ On the other hand, as a result of the increase in *d*, the LSPR absorption intensity increases while the Au surface area decreases. The balance between them determines the optimum *d* value.

In summary, we have shown that visible-light irradiation of Au/rutile TiO₂ in amines yields the corresponding imines on a synthetic scale with high selectivity (>99%) under solvent-free conditions at 298 K. The information about the strong support effects and Au particle size effects on the photocatalytic activity should greatly contribute to the material design for plasmon photocatalysts.

■ ASSOCIATED CONTENT

Supporting Information

Experimental details, properties of the supports and Au NPs (Table S1, Figure S1), time course for the amine oxidation

(Figure S2), amine oxidation (Table S2), and PCP curves (Figure S3). This material is available free of charge via the Internet at <http://pubs.acs.org>.

■ AUTHOR INFORMATION

Corresponding Author

*E-mail: h-tada@apch.kindai.ac.jp.

Notes

The authors declare no competing financial interest.

■ REFERENCES

- (1) Cozzi, P. G. *Chem. Soc. Rev.* **2004**, *33*, 410.
- (2) Murahashi, S. *Angew. Chem., Int. Ed.* **1995**, *34*, 2443.
- (3) Nicolaou, K. C.; Mathison, C. J. N.; Montagnon, T. *Angew. Chem., Int. Ed.* **2003**, *42*, 4077.
- (4) Mukaiyama, T.; Kawana, A.; Fukuda, Y.; Matsuo, J. *Chem. Lett.* **2001**, *30*, 390.
- (5) Furukawa, S.; Ohno, Y.; Shishido, T.; Teramura, K.; Tanaka, T. *ACS Catal.* **2011**, *2*, 1150.
- (6) Schümperli, M. T.; Hammond, C.; Hermans, I. *ACS Catal.* **2012**, *2*, 1108.
- (7) Kubacka, A.; Fernandez-Garcia, M.; Colon, G. *Chem. Rev.* **2012**, *112*, 1555.
- (8) Wen, B.; Ma, J.-H.; Chen, C.-C.; Ma, W.-H.; Zhu, H.-Y.; Chao, J.-C. *Sci. China, Chem.* **2011**, *54*, 887.
- (9) Tian, Y.; Tatsuma, T. *J. Am. Chem. Soc.* **2005**, *127*, 7632.
- (10) Silva, C. G.; Juárez, R.; Marino, T.; Molinari, R.; García, H. *J. Am. Chem. Soc.* **2011**, *133*, 595.
- (11) Yuzawa, H.; Yoshida, T.; Yoshida, H. *Appl. Catal., B* **2012**, *115–116*, 294.
- (12) Alvaro, M.; Cojocar, B.; Ismail, A. A.; Petrea, N.; Ferrer, B.; Harraz, F. A.; Parvulescu, V. I.; García, H. *Appl. Catal., B* **2010**, *99*, 191.
- (13) Primo, A.; Marino, T.; Corma, A.; Molinari, R.; García, H. *J. Am. Chem. Soc.* **2011**, *133*, 6930.
- (14) Liu, Z.; Hou, W.; Pavaskar, P.; Aykol, M.; Cronin, S. B. *Nano Lett.* **2011**, *11*, 1111.
- (15) Wand, P.; Huang, B.; Qin, X.; Zhang, X.; Dai, Y.; Wei, J.; Whangbo, M.-H. *Angew. Chem., Int. Ed.* **2008**, *48*, 7931.
- (16) Wang, P.; Huang, B.; Dai, Y.; Whangbo, M.-H. *Phys. Chem. Chem. Phys.* **2012**, *14*, 9813.
- (17) Kowalska, E.; Abe, R.; Ohtani, B. *Chem. Commun.* **2009**, 241.
- (18) Naya, S.; Inoue, A.; Tada, H. *J. Am. Chem. Soc.* **2010**, *132*, 6292.
- (19) Tsukamoto, D.; Shiraishi, Y.; Sugano, Y.; Ichikawa, S.; Tanaka, S.; Hirai, T. *J. Am. Chem. Soc.* **2012**, *134*, 6309.
- (20) Naya, S.; Teranishi, M.; Isobe, T.; Tada, H. *Chem. Commun.* **2010**, *46*, 815.
- (21) Ide, Y.; Matsuoka, M.; Ogawa, M. *J. Am. Chem. Soc.* **2010**, *132*, 16762.
- (22) Zheng, Z.; Huang, B.; Qin, X.; Zhang, X.; Dai, Y.; Wei, J.; Whangbo, M.-H. *J. Mater. Chem.* **2011**, *21*, 9079.
- (23) Kimura, K.; Naya, S.-i.; Jin-nouchi, Y.; Tada, H. *J. Phys. Chem. C* **2012**, *116*, 7111.
- (24) Tada, H.; Kiyonaga, T.; Naya, S.-i. *Metal Oxide-Supported Gold Nanoparticles*; Lambert Academic Publishing, 2012.
- (25) *Handbook of Chemistry and Physics*, 89th edition; Lide, D. R., Ed.; CRC Press: Boca Raton, FL, 2008.
- (26) Lang, X.; Ma, W.; Zhao, Y.; Chen, C.; Ji, H.; Zhao, J. *Chem.—Eur. J.* **2012**, *18*, 2624.
- (27) Ferretto, L.; Glisenti, A. *Chem. Mater.* **2003**, *15*, 1181.
- (28) Hoft, R. C.; Ford, M. J.; McDonagh, A. M.; Cortie, M. B. *J. Phys. Chem. C* **2007**, *111*, 13886.
- (29) Maruska, H. P.; Ghosh, A. K. *Sol. Energy* **1978**, *20*, 443.
- (30) *Denki Kagaku Binran*, Electrochemical Society of Japan: Maruzen, Tokyo, 2000.
- (31) Scaife, D. E. *Sol. Energy* **1980**, *25*, 41.